

Article

# A Multi-Scale Approach for Improved Characterization of Surface Water—Groundwater Interactions: Integrating Thermal Remote Sensing and in-Stream Measurements

Dilge Varli and Koray K. Yilmaz \* 

Department of Geological Engineering, Middle East Technical University, Ankara 06800, Turkey; dilge.varli@metu.edu.tr

\* Correspondence: yilmazk@metu.edu.tr; Tel.: +90-312-210-2689

Received: 23 May 2018; Accepted: 22 June 2018; Published: 27 June 2018



**Abstract:** The interaction between surface water and groundwater is recognized as a key process for effective management of water resources. However, scale dependency and spatial heterogeneity of the processes at the interface are limiting factors in the characterization of this process. A hierarchical, multi-scale methodology has been devised and demonstrated to effectively and efficiently characterize the surface water-groundwater interaction along a 2-km reach in Kirmir stream, Turkey. Our methodology starts with investigation of geological information at the regional scale. At the intermediate scale, thermal infrared imagery is utilized to pinpoint groundwater seepage locations. Discharge measurements helped to understand the gains/losses. Point scale measurements including vertical hydraulic gradients, streambed vertical/horizontal temperature profiles and electrical conductivity profiles are investigated to characterize spatio-temporal variation in the vertical fluid fluxes. The results indicated that the study reach can be separated into three sections; upstream losing section, downstream gaining section and mid-section with a seasonally variable character. Moreover, dam operation was found to control the exchange process—a rapid rise in the river stage resulted in temporary reversal of the exchange processes. Analysis of chloride concentrations indicated that the lower confined aquifer is likely the source for the seepage at a fault-controlled section of the streambed.

**Keywords:** stream-groundwater interaction; hierarchical approach; heat flux; water quality; thermal infrared imagery

## 1. Introduction

Groundwater and surface water are hydraulically connected with each other [1–3]. Their interaction occurs at multiple spatio-temporal scales and has significant implications, for example, on effective management of water resources [4,5] and the ecological status of both river corridor [6,7] and the groundwater bodies [5,8]. As such, the European Union Water Framework Directive (WFD; 2000/60/EC) outlines an approach for the management of water resources by focusing on interaction between groundwater bodies, groundwater dependent terrestrial ecosystems and surface water bodies. Hence, studies focusing on monitoring and characterization of the exchange fluxes between surface water and groundwater bodies are gaining increasing attention [9–11].

The direction and degree of interaction between groundwater and surface water are mainly controlled by geology, geomorphology, topography, climate, and the position of surface water body and water table with respect to each other [2,12,13] and often show significant variation in space and time. For this reason, the exchange processes are complex and difficult to characterize. As scale

changes, interaction changes from shallow hyporheic interactions [14] to meander necks in regional scales [15] or regional exchanges at the catchment scale [4]. The distribution of subsurface flow paths in streambeds also changes as a function of scale-dependent physical processes [16]. Hence, a detailed field investigation is needed to understand and quantify groundwater-stream interaction [17,18] with data and methods that are appropriate for the scale of interest [19–22].

Choosing an appropriate technique to quantify the interaction process depends on the purpose, temporal and spatial scales, limitations and uncertainties [20]. Direct measurement of water fluxes is provided by seepage meters [23], which provide only point-scale estimates [24–27]. One of the most common techniques to quantify exchange fluxes through groundwater-stream interface is to apply Darcy's equation using hydraulic gradient and conductivity information. This approach provides only larger scale estimates depending on the positions of piezometers when compared to seepage meters [28]. Also, vertical hydraulic conductivity values through the streambed may vary within a reach [21]. As a result, vertical fluxes along the streambed are significantly heterogeneous [29,30]. Therefore, application of multiple methods at a range of scales is expected to improve the understanding of groundwater-surface water interaction processes [9,21,22].

To overcome such problems in quantifying the exchange processes, we developed a hierarchical approach where we integrated geological information and remotely sensed stream surface temperature measurements with a set of in-stream measurements representing a cascade of scales; from regional to point. The hierarchical approach starts with the identification of stream reaches with a potential interaction between groundwater and surface water at a regional scale using geological/geomorphological information; then thermal infrared imagery is utilized as an intermediate scale to rapidly screen areas of groundwater inflow, followed by in-situ measurements at the local scale for detailed characterization. Lastly, chloride concentrations are used as a tracer to identify the source aquifer(s) feeding the stream. Hence, in this study, we propose a hierarchical, multi-scale framework that enables cost-effective and efficient identification and quantification of spatially and temporally variable groundwater contributions to streams. The proposed methodology is demonstrated by characterizing the groundwater-surface water exchange processes along a 2-km reach of the Kirmir Stream in Ankara, Turkey.

## 2. Study Area

### 2.1. Location and Surface Water Resources

The study was carried out along a 2.1-km long reach of the Kirmir Stream that flows in northeast-southwest direction and is located 55 km northwest of Ankara, Turkey (Figure 1). The study area is surrounded by a steep and rugged topography. Elevation ranges between 760 m and 780 m along the study reach. A meteorological station is situated 4.3 km south of the study area. Kirmir Stream is an important water resource for the city of Ankara, supplying water to the city through Akyar Dam, Egrekaya Dam and Doganozu Dam which are located upstream of the study reach. The study reach is located where major faults—Kizilca, Kirmir 2 and Demircioren—are situated nearby the stream channel, thus increasing the potential for connection between groundwater and surface water. There is no surface water input along the study reach; therefore, any change in streamflow along the reach is likely due to the exchange between surface water and groundwater.

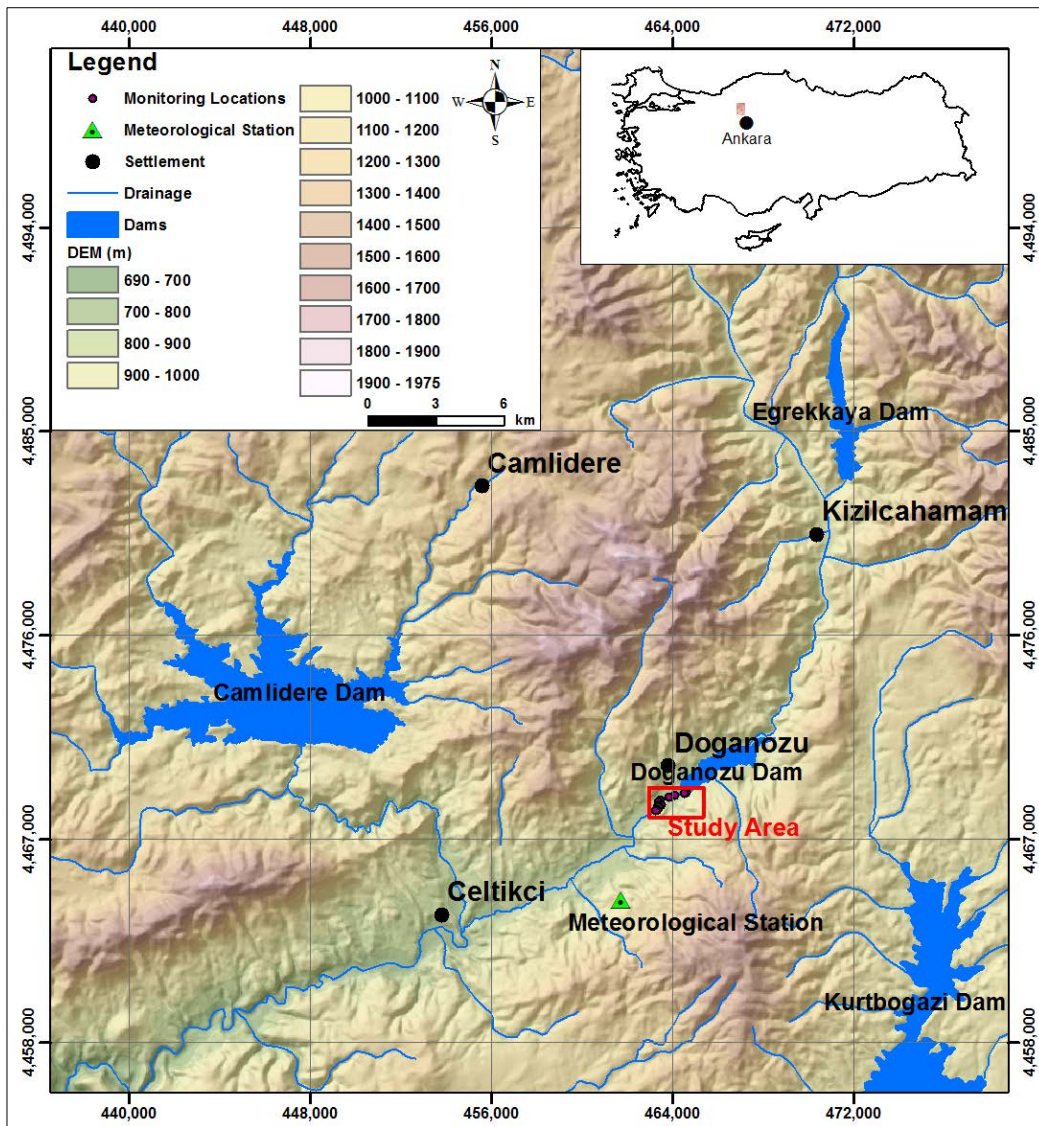


Figure 1. Regional view of the study area.

The study reach starts immediately downstream of Doganozu Dam (Figure 2); therefore, the effect of dam on the exchange processes can be investigated. Fourteen monitoring locations were setup along the reach and named as S1-P, S2-P, S3-P, S4-P, S6-P, S7-P, S9-P, S10-P, S12-D, S13-D, S14, S15, S16-D and S17-D. S1-P and S17-D sites mark the most upstream and downstream locations, respectively, and are situated 2.1 km apart from each other. The letters P and D denote piezometer and discharge measurement sites, respectively.

## 2.2. Geology and Hydrogeology

The study area is located on the southern margin of a volcanic terrain, which is known as “Galatian Volcanic Province” (GVP). GVP is located between Cretaceous accretionary prism and the North Anatolian Fault Zone (NAFZ). The geological units exposed around the study area are classified as Miocene aged basement volcanics and Celтикci formation, Plio-Quaternary units, and Quaternary alluvium from bottom to top [31] (Figure 3). Celтикci formation is divided into seven units.

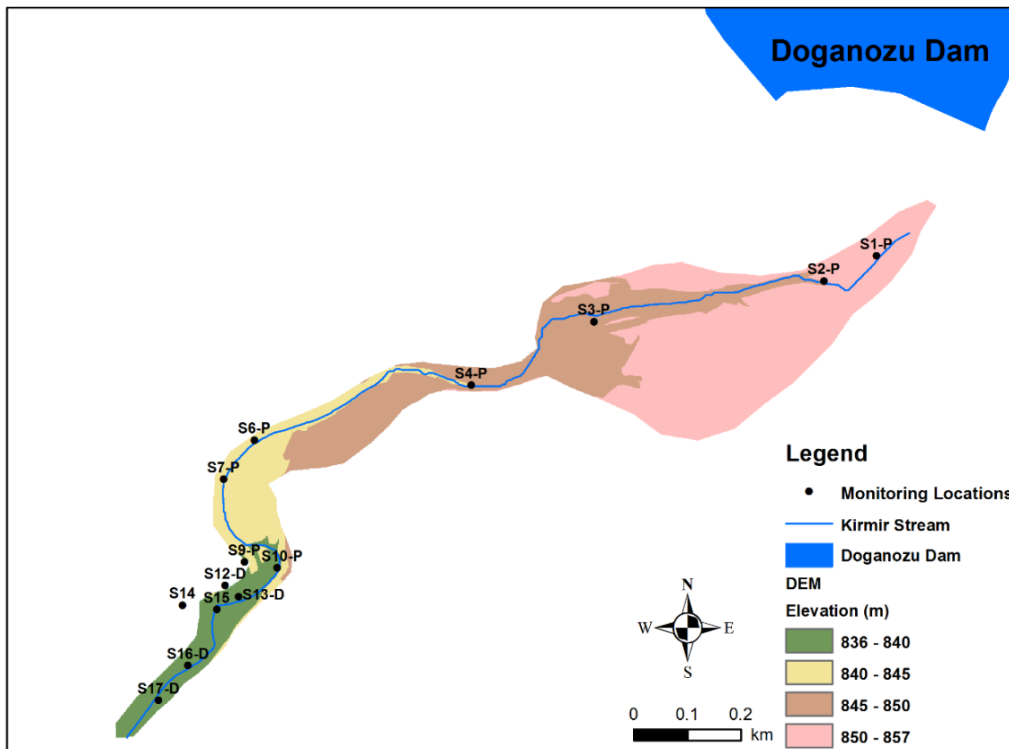


Figure 2. Monitoring locations along the study reach.

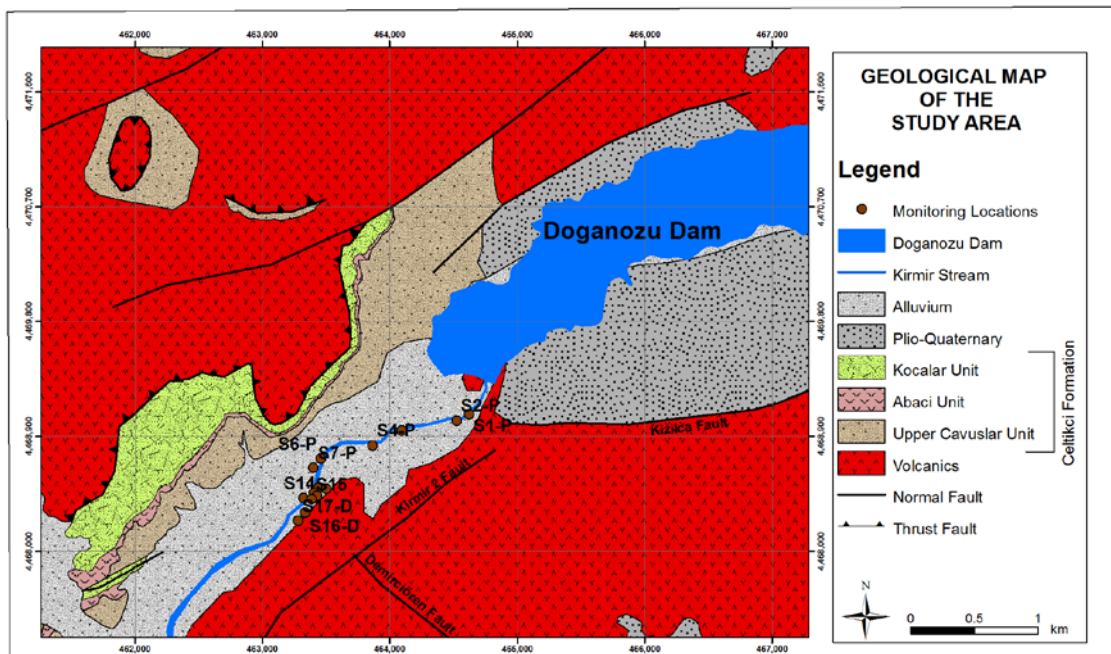


Figure 3. Geological map of the study area [31].

These are, from bottom to top, Bostantepe, Lower Cavuslar, Upper Cavuslar, Abaci, Kocalar, Aktepe and Bezci units. Among these, basement volcanics, Upper Cavuslar unit, Abaci unit, Kocalar unit of the Celtikci formation, Plio-Quaternary units and Quaternary alluvial deposits. Miocene aged volcanics include pyroclastics, tuffs and lava flows, Upper Cavuslar unit includes marl—claystone alternation and mudrocks with sandstones and tuffs, Abaci unit is a single ignimbrite (tuff) layer,

Kocalar unit is characterized by mudrocks with sandstone beds and tuff layer and lastly sandstone, siltstone and conglomerates occur as Plio-Quaternary units. At the top, Quaternary aged alluvium is observed. Normal and thrust faults have been identified near the study reach.

In the region, three major aquifer systems were identified by Yazıcıgil et al. [32]. Quaternary aged alluvium along Kirmir stream forms an unconfined aquifer with an approximate thickness of 20–25 m. Kocalar unit (mudrocks, sandstones and tuffaceous layers), Aktepe unit (limestones and dolomitic mudrocks), Bezci unit (sandstones and siltstones) of the Celtikci formation form the upper unconfined aquifer system; whereas Upper Cavuslar unit represents the lower confined aquifer system.

### 3. Methods

Our methodology is based on a hierarchical multi-scale approach. At the first stage, geological and geomorphological information, such as geological units/structures (i.e., faults) and changes in streambed slope have been investigated to identify stream reaches that have potential of groundwater-surface water interaction. In the light of this information, field investigations were performed spanning reach to point scales.

#### 3.1. Measurement of Water Skin Temperatures Using Thermal Camera

Heat flows continuously between surface water and adjacent ground water providing an opportunity to use heat as a natural tracer of interaction [33]. The premise is that, groundwater temperatures are relatively constant throughout the year, whereas stream temperatures vary daily and seasonally [20] in response to change in air temperature. We used a handheld thermal infrared camera to quickly detect and characterize thermal anomalies in shallow surface water skin temperatures that in turn could potentially indicate groundwater seepage zones into the streambed. The camera utilized is an Optris® PI160 having a resolution of  $160 \times 120$  pixels, wavelength range of 7.5–13  $\mu\text{m}$  and a pixel-to-pixel thermal accuracy of 0.08 K with a lens field of view of  $23^\circ \times 17^\circ$ . Starting from immediately downstream of the Doganozu Dam, we investigated the Kirmir Stream skin temperatures with TIR images taken on 9 and 24 September 2014, 15 January 2015 and 26 February 2016. In the procedure, we walked along the stream while monitoring real time thermal and visible imagery gathered simultaneously through the thermal camera and a regular camera mounted on a handheld platform. We utilized the information gathered from this rapid survey in planning other field methods.

#### 3.2. Nested Piezometers

Sixteen piezometers (7 nested and 2 single) were installed within the streambed using a sledgehammer to obtain hydraulic gradient information. Each piezometer consists of stainless steel pipe with an inner diameter of 32 mm and a 20 cm long perforated section. The shallow piezometers are 185 cm in length, while the deep piezometers varied between 270 cm and 285 cm depending on the locations. The mid-point of the perforated sections represents a depth into the streambed sediments that varied between 54 cm and 69 cm for shallow piezometers and 147 cm to 176 cm for deep piezometers.

Nested piezometers—S4-P, S6-P, S7-P and S10-P—were installed on 25 September and 16 October 2014, respectively. The nested piezometers at S1-P, S2-P, S3-P and 2 single piezometers in S9-P were installed on 21 November 2014. S9-P represents two deep piezometers placed at the opposing sides of a pond. Bi-weekly water level measurements were taken from all piezometers between 16 October 2014 and 19 November 2015 using a Solinst® level meter (Model 107 TLC Meter).

Vertical hydraulic gradient values were calculated for both nested and single piezometers. The sign of the vertical hydraulic gradient indicates the direction of water flow within the streambed. In this study, a positive gradient value indicates downwelling and a negative value indicates upwelling flux respectively.

### 3.3. Differential Discharge Measurements

Streamflow discharge measurements were performed bi-weekly between 9 September 2014 and 14 September 2015 (15 times) using a current meter (FP111 Global Water Flow Probe). Initially, S12-D, S13-D and S17-D locations were designated as discharge measurement locations. As the study progressed, locations S16-D, S3-P and S6-P were also included to better characterize the groundwater-surface water exchange along the reach. S3-P and S17-D are the most upstream and downstream discharge measurement locations, respectively. S12-D and S13-D are located on two branches of the stream that merge and flow towards S16-D (see Figure 2). Due to this reason, the sum of discharge at these locations was included in the analysis. Temporal variation in discharge values (given as L/s and equals to  $1 \times 10^{-3} \text{ m}^3/\text{s}$  in SI units) between each location was investigated to understand the gaining and losing sections of the Kirmir Stream. Note that each measurement campaign was performed within a day to remove temporal bias across measurement locations.

### 3.4. Vertical Water Flux Calculations from Streambed Temperature Profiles

Vertical water flux values in the streambed were calculated from temperature profiles using the amplitude ratio ( $A_r$ ) method [34]:

$$v_{Ar} = \frac{2K_e}{\Delta z} \ln A_r + \sqrt{\frac{\alpha + v^2}{2}} \quad (1)$$

$$K_e = \left( \frac{\lambda_o}{C} \right) + \beta |v_f| \quad (2)$$

where  $K_e$  is effective thermal diffusivity of the saturated sediment ( $\text{m}^2/\text{s}$ ),  $A_r$  is the ratio of amplitudes between a lower and an upper temperature signal (unitless),  $\Delta z$  is the vertical distance between the measurement points (m),  $\alpha = \sqrt{v^4 + (8\pi K_e/P)^2}$ ,  $P$  is the period of temperature variations,  $v$  is the rate of penetration of the thermal front and proportional to the fluid velocity ( $v_f$ ) by  $v = v_f / \gamma$  where  $\gamma$  is the ratio of streambed and fluid volumetric heat capacity (fluid velocities are calculated using the latter relationship),  $\lambda_o$  is the baseline thermal conductivity of the saturated sediment ( $\text{cal}/(\text{s}\cdot\text{cm}\cdot^\circ\text{C})$ ),  $\beta$  is thermal dispersivity (m). In the procedure, the VFLUX program provided by [34] was utilized. This program uses temperature time series, the vertical distance between temperature loggers, total porosity (taken as 0.28) and thermal properties of the sediment and water as inputs: thermal dispersivity (0.001 m), thermal conductivity ( $0.0045 \text{ cal}/(\text{s}\cdot\text{cm}\cdot^\circ\text{C})$ ), volumetric heat capacity of the sediment ( $0.5 \text{ cal}/(\text{cm}^3\cdot^\circ\text{C})$ ) and lastly volumetric heat capacity of the water ( $1.0 \text{ cal}/(\text{cm}^3\cdot^\circ\text{C})$ ). These values were selected based on literature [34]. Other thermal methods also exist in the literature that utilize vertical temperature measurements at various depths in the streambed to quantify the exchange fluxes (e.g., [9,35,36]). Briggs et al. (2014) [37] provides guidance on the use of diurnal temperature signals for upwelling systems.

Streambed temperatures at different depths were measured using Thermochron i-Button<sup>®</sup> temperature data loggers (Maxim Integrated<sup>®</sup> Model No. DS1922L-F5). This model has a temperature range of  $-40^\circ\text{C}$  to  $+85^\circ\text{C}$ , with an accuracy and resolution of  $\pm 0.5^\circ\text{C}$  and  $0.0625^\circ\text{C}$ , respectively. i-Buttons were installed at S3-P, S4-P and S16-D locations representing upstream, middle and downstream sections of the study reach, respectively. Each location contained two i-Buttons that were mounted on a wooden dowel ( $30 \text{ cm} \times 4 \text{ cm} \times 2.8 \text{ cm}$ ) with a separation distance representing different depths in the streambed. The procedure included the following steps: (1) each i-Button was coated with thin PlastiDip<sup>®</sup> (Performix) rubber cover for waterproofing and was placed into one of the two hollows opened in each dowel; (2) A stainless steel washer was placed as a cap over each i-Button for protection while ensuring thermal connection with sediments; (3) Lastly, the dowel was driven into the streambed so that the top and bottom i-Button remained 5 cm and 20 cm below the streambed. i-Buttons were left in the study area for three different time periods. Measurement period 1 spans through 16–25 March 2015 for locations S3-P and S4-P and 16 March to 27 April 2015 for

location S16-D. Measurement period 2 spans from 12 July to 2 August 2015 for all locations. The last measurement period spans through 5–13 September 2015 for S4-P and S16-D. Note that in the second and the third installations, the bottom i-Button was inserted 15 cm into the streambed instead of 20 cm. For each measurement period, i-Buttons were programmed to record streambed temperatures at 15-min intervals. For the first measurement period, i-Buttons at S16-D had to be left in the field for a longer period, because the site was inaccessible due to reservoir water release on 26 March 2015.

### 3.5. Measurement of Temperature, Electrical Conductivity and Chloride Concentrations

Temperature and electrical conductivity (normalized to 25 °C) values were measured from stream water at all monitoring sites (S1-P to S17-D) and at each piezometer using a Solinst® level meter (Model 107 TLC Meter). All measurements were performed bi-weekly between October 2014 and November 2015. Note that S15 is located along the main channel and downstream of the point where two branches S12-D and S13-D merge. Hence, two measurements were performed in S15 and were denoted as S15-12 and S15-13, separately representing these branches. S17-D was investigated as S17-D-I and S17-D-II; these sites refer to minor branching nearby S17-D.

To investigate the variation in chloride ( $\text{Cl}^-$ ) concentrations, water samples representing both surface water (a few meters upstream and downstream of each site) and deep piezometers, where available, were taken on 4 August 2015 from sites S2-P, S4-P, S6-P, S10-P, S12-D, S13-D, S16-D and S17-D and analyzed using ion chromatography. Solute mass balance calculations using the Chloride concentrations and concurrent stream discharge values were utilized to understand the contribution of groundwater to the study reach:

$$Q_{\text{gw}} = (Q_2 C_2 - Q_1 C_1) / C_{\text{gw}} \quad (3)$$

where  $Q_1$ ,  $Q_2$  and  $Q_{\text{gw}}$  represents the flow upstream, flow downstream and groundwater inflow.  $C_1$ ,  $C_2$  and  $C_{\text{gw}}$  represent the concentration of conservative chloride ion in upstream and, downstream surface water and groundwater, respectively.

## 4. Results

### 4.1. Reach Scale: Water Skin Temperatures Using Thermal Infrared Camera

High resolution TIR imagery acquired with the handheld camera enabled rapid identification of groundwater seepage zones that are detectable on the surface water skin and along the streambank. In summer (winter), cold (warm) anomalies in the surface water potentially indicate locations where groundwater seep occurs through the streambed.

Figure 4 shows a sample TIR imagery taken at location S10-P on 26 February 2016; on a cold winter day (air temperature is 8.3 °C during image acquisition). Warmer groundwater (21 °C) seeping into the colder surface water (8 °C) can be clearly seen in TIR spectrum with a well-developed interface.

Figure 4c,d shows the TIR and visible images taken at site S15 on 15 January 2015 (winter) with an air temperature of 7.2 °C. This site marks the confluence of two stream branches where S12-D and S13-D sites are located (see labels on the figure). It is clear from this imagery that the representative temperature of S12-D branch (8.3 °C) was close to the air temperature (7.2 °C), indicating surface water character, whereas the representative temperature of S13-D branch (15.1 °C) was significantly warmer. Note that groundwater seepage site S10-P is situated immediately upstream of S13-D.

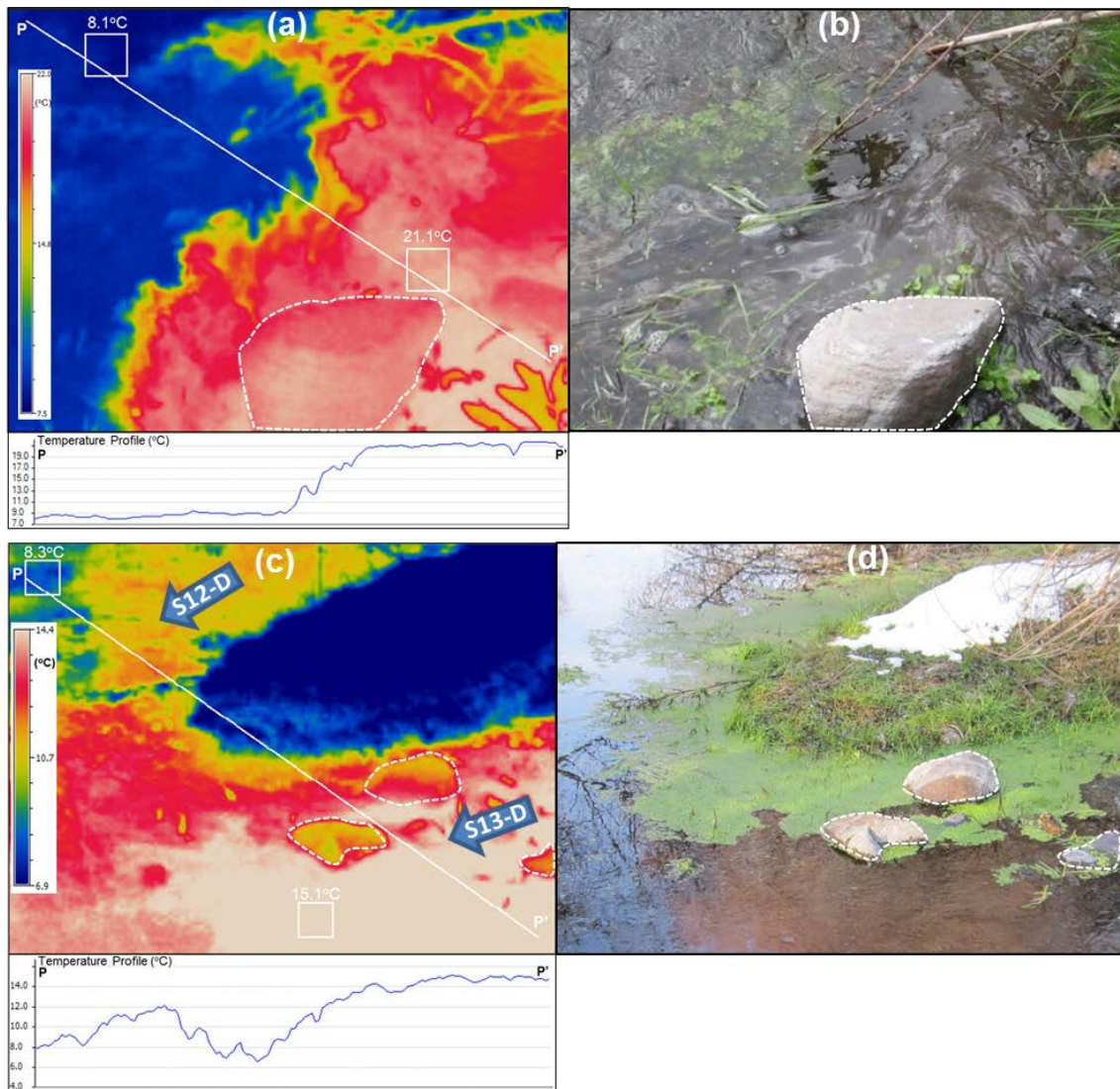


**Figure 4.** (a) A sample TIR imagery indicating groundwater seepage (warmer) close to S10-P location; (b) visible imagery of the same location; (c,d) same as (a,b) but for a location where two stream branches with different surface water skin temperatures merge. Note: In TIR imagery, the diagonal line is the temperature profile line and each rectangle denote the representative averaging areas with average temperature indicated on top.

#### 4.2. Point Scale: Analysis of Vertical Hydraulic Gradient (VHG) Values from Piezometers

Piezometers were installed at eight locations to measure temporal variation in VHG values. VHG measurements indicated that the study reach could be classified into three distinct sections based on the character of the water exchange (Figure 5). The most upstream section (S1-P, S2-P and S3-P) is characterized by consistent positive VHG values (hydraulic head values of deep piezometers are lower compared to shallow piezometers and surface water) throughout the observation period—indicating a losing section with downward movement of surface water regardless of the season. The mid-section (includes S4-P, S6-P and S7-P) corresponds to a section that is sometimes gaining and other times losing (negative and positive VHG values). In winter, VHG values are close to zero indicating no major interaction; however, starting from spring and summer, VHG values become more negative, indicating stronger groundwater discharge into the stream and consequently, seasonal dependency. Along this reach, all piezometer locations consistently indicate that the major groundwater discharge occurs in the May–July period. The most downstream nested piezometer location, namely, site S10-P, is

characterized by consistently negative VHG values, representing a gaining section regardless of the season. Among all sites, site S10-P is characterized by the most negative VHG values regardless of the season. The seasonal variation of VHG at site S10-P indicates that the most significant upwelling period is the May–July 2015 period; similar to the previous section.

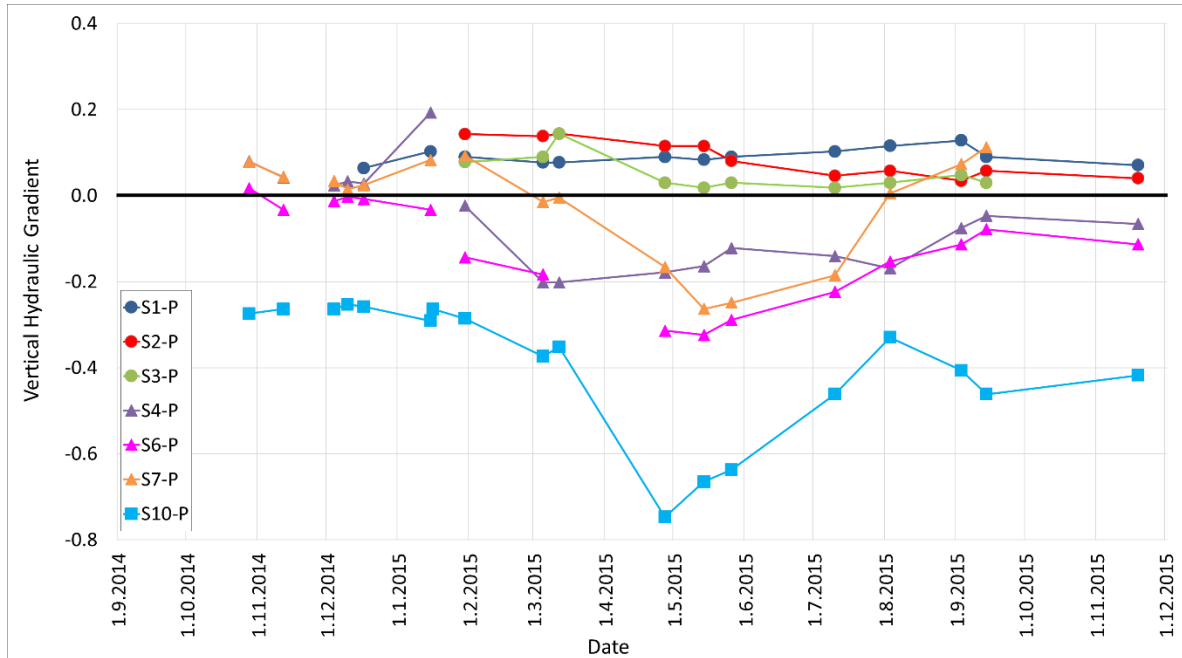


Figure 5. VHG variation in time for each piezometer location.

One potential reason controlling the direction of the exchange processes along these sections is the variation in streambed elevation because topography has fundamental importance in controlling the water exchange along the streambed [14]. Groundwater typically discharges to surface water bodies where the slope of the water table changes suddenly, e.g., [2]. Figure 6 shows the streambed elevation profile along the study reach. Note that the elevation drops more than 14 m along the study reach with steeper slope of the streambed between sites S3-P and S10-P. The site S10-P representing the lowest streambed elevation, where a piezometer is installed, has the highest VHG values.

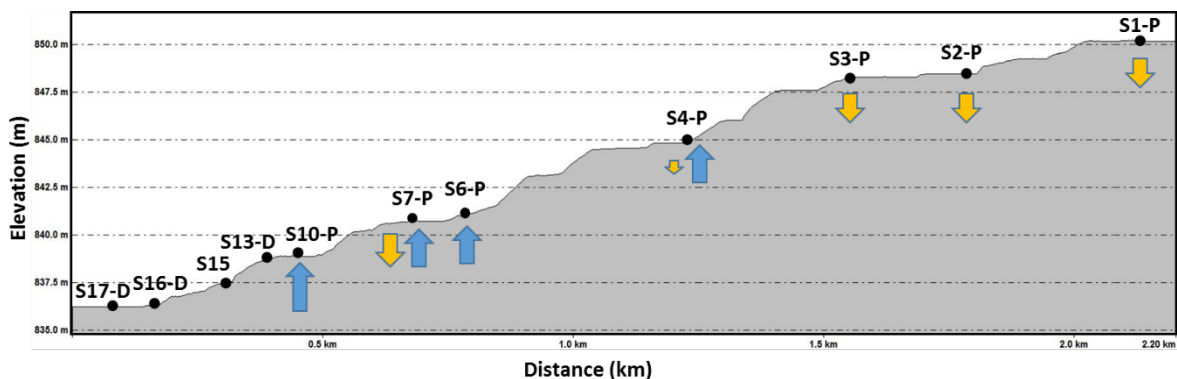
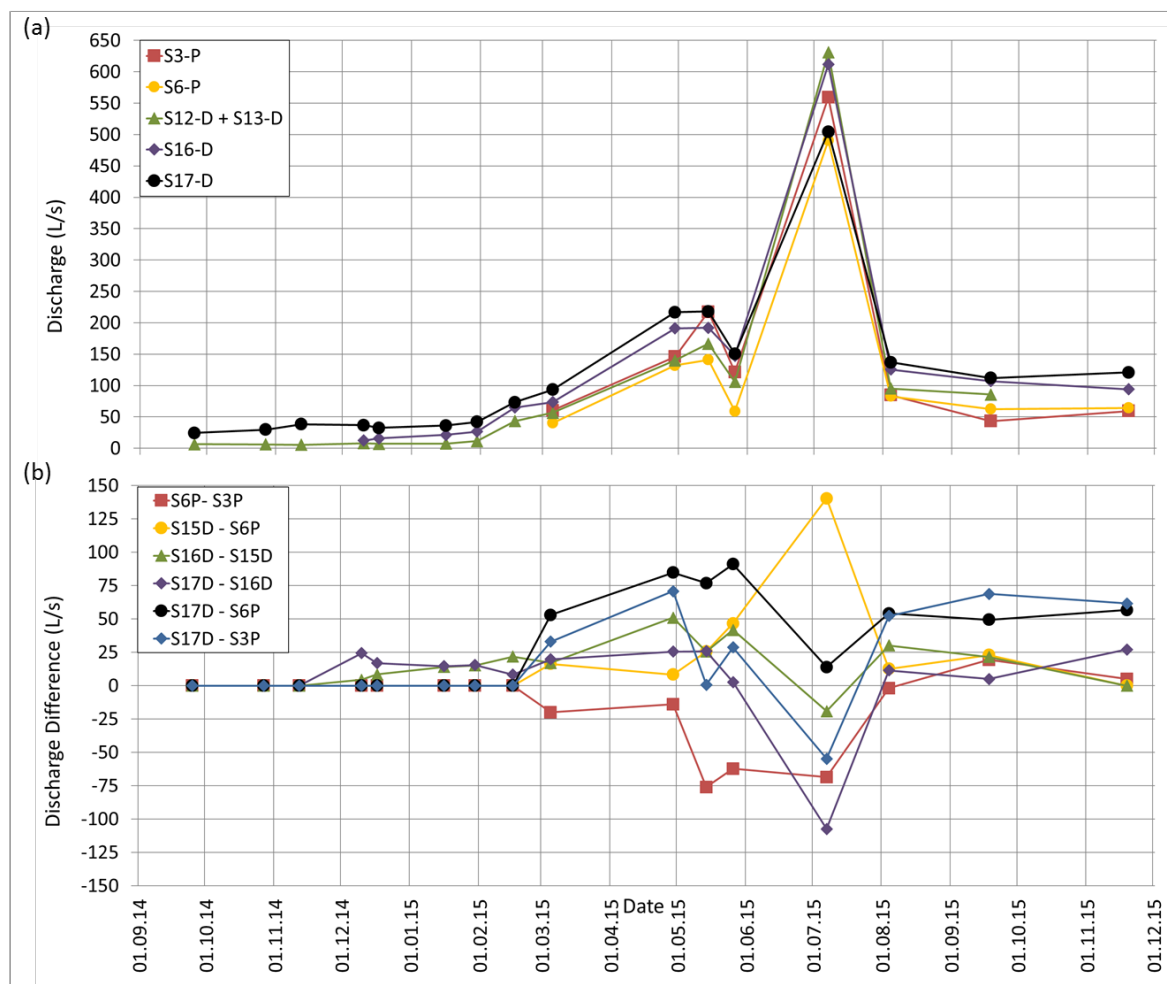


Figure 6. Streambed elevation profile along the study reach. The arrows indicate the direction and the approximate magnitude of the exchange process.

### 4.3. Temporal Variation in Stream Discharge

Figure 7a,b shows the variation in stream discharge at the monitoring sites and differences between adjacent sites (positive values indicate increasing discharge downstream), respectively.



**Figure 7.** Variation in (a) stream discharge at the monitoring sites; (b) difference in discharge between adjacent sites (positive values indicate increasing discharge in the downstream direction).

Figure 7a shows that the discharge generally increased downstream. During spring (March–June 2015), the discharge at the most upstream site, namely S3-P, was higher than at S6-P. This could possibly be explained by the fact that part of the downwelling surface water at S3-P upwells after the downstream site S6-P; note that discharge at S15 is higher than at S6-P, supporting this argument. The peak discharge values in July 2015 is due to the release of reservoir water, and the uncertainty in peak discharge measurements are relatively high at this time due to turbulent conditions. In summary, the discharge measurements indicate that the study reach gains water when moving towards downstream along the study reach.

Figure 7b indicates that Kirmir stream gains water through the streambed in a spatially varying manner. The most significant increase in discharge occurs between S17-D (the most downstream site) and S6-P (first discharge measurement location with a gaining character) with values between 50 L/s and 91 L/s. The water gain is more significant between these locations compared to the section between S17-D and S3-P (most upstream location where discharge measurements exist). As explained earlier, S3-P is located along a losing reach and part of the water entering the streambed around this site likely upwells after site S6-P. This situation is also evident from the negative discharge differences

between S6-P and S3-P. On the contrary, the discharge measured in S17-D is lower than the discharge measured at S3-P, S15-D and S16-D on 7 July 2015. This reversal is possibly due to the reservoir water release from Doganozu Dam. It is likely that the increase in surface water stage during dam water release turns the stream into a dominantly losing stream along the study reach. After this date, discharge in S17-D is higher again and the difference from the S3-P ranges between 52.3 L/s and 68.7 L/s.

#### 4.4. VFLUX Results

##### 4.4.1. Streambed Temperatures

Diurnal fluctuations in streambed temperatures were recorded at sites S3-P, S4-P and S16-D at two different depths for three different measurement periods (Table 1).

**Table 1.** Maximum and minimum values of the streambed temperatures at monitoring sites S3-P, S4-P and S16-D for each measurement period.

Site	Measurement Period	Depth (cm)	Streambed Temperature		
			Max (°C)	Min (°C)	Difference (°C)
S3-P	16–25 March 2015	5	9.83	5.26	4.58
		20	7.98	7.23	0.75
	12 July–2 August 2015	5	27.65	19.71	7.94
		15	25.88	21.25	4.63
S4-P	16–25 March 2015	5	13.70	12.32	1.38
		20	14.56	13.37	1.19
	12 July–2 August 2015	5	15.62	14.86	0.75
		15	15.47	14.53	0.94
	5–13 September 2015	5	17.12	16.81	0.31
		15	16.97	16.72	0.25
S16-D	16 March–27 April 2015	5	16.81	7.08	9.72
		20	17.68	8.15	9.53
	12 July–2 August 2015	5	18.40	18.08	0.31
		15	18.38	18.07	0.31
	5–13 September 2015	5	18.46	18.40	0.06
		15	18.38	18.32	0.06

Among the three measurement sites, the highest temperature value (27.7 °C at 5 cm depth in July–early August 2015 period) and the lowest temperature value (5.3 °C at 5 cm depth in March) were measured at location S3-P (Table 1). Significant variation in streambed temperatures in response to air temperatures indicates that S3-P is located in the losing section of the study reach. At sites S4-P and S16-D the temperature at two different depths are similar to each other for September 2015 period and July–August–September 2015 periods, respectively. At site S4-P, the temperature values at two different depths measured in March are not as similar as other measurement periods, but the difference is not more than 1.4 °C. Therefore, it can be concluded that during the measurement period, sites S4-P and S16-D are under the influence of the upwelling water from the streambed and hence are not affected significantly by the diurnal changes in air temperature.

In July, August and September, streambed temperatures at site S16-D are relatively stable with values around 18 °C; note that the difference between maximum and minimum temperatures is less than 0.5 °C. However, there is a significant difference (8.5 °C) between maximum and minimum temperature values for the March–April 2015 period in S16-D. Figure 8b shows the streambed temperature variation at site S16-D at two depths for this time period. At the end of the first

measurement period, site S16-D was inaccessible due to reservoir water release on 26 March 2015 and i-Buttons at S16-D were left for a longer period compared to loggers at sites S3-P and S4-P. Apart from the diurnal variations in streambed temperatures, a periodic change in the temperature values reflects the reservoir operation (marked as Segment I through Segment V in Figure 8b). During reservoir water release (e.g., Segment II), the temperature values at both depths decreased significantly (more significantly at the deeper section) and reached values that are close to the air temperature, indicating the influence of the surface water and hence decrease in upwelling flux. Figure 8b shows that the reservoir operation was halted on 2 April and re-started on 9 April 2015. The streambed temperature difference at two depths was more pronounced in Segment IV compared to Segment II indicating less surface water during the former segment. Note that after the release of reservoir water halted, streambed temperature at 20 cm depth reached an almost stable value of around 17 °C, with higher temperature values than air temperature values and less diurnal variation compared to the temperature at 5 cm depth.

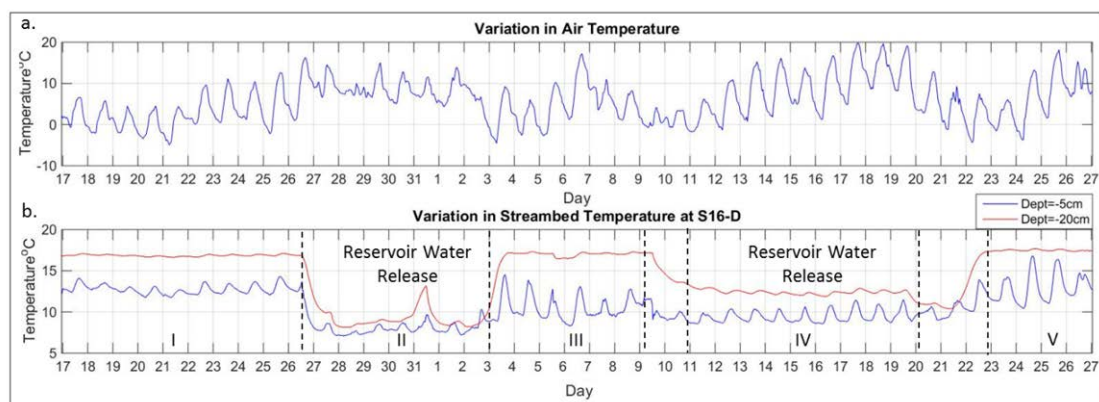


**Figure 8.** (a) Variation in air temperature; (b) variation in streambed temperature during March–April period at two different depths at site S16-D. Note that the measurement period is divided into five segments based on reservoir water release.

#### 4.4.2. Vertical Fluid Flux Values

Vertical fluid flux values were estimated from the diurnal variations in streambed temperature values at two different depths using the amplitude ratio method of Hatch et al. [34]. Note that the diurnal variation in temperature values should be greater than the sensor precision (0.0625 °C for the i-Button model used in this study) for the flux values to be reliable. For sites S4-P and S16-D, the amplitude of diurnal temperature variations at 20 cm depth was less than the sensor precision during the July–August and September 2015 periods. Thus, flux values were deemed unreliable for these sites and periods. Note, however, that lack of diurnal temperature variations at this depth is an indication of strong upwelling flux at these sites.

Figure 9 summarizes the distribution of vertical flux for sites S3-P, S4-P and S16-D for 16–25 March, 12 July–2 August and 16 March–27 April 2015 measurement periods. It can be seen that both S3-P and S4-P sites are characterized by upwelling (negative) flux with values generally ranging between  $-4 \times 10^{-6}$  m/s and  $-5 \times 10^{-6}$  m/s during March 2015. In July–August 2015 period, S3-P is characterized by downwelling flux (positive values).

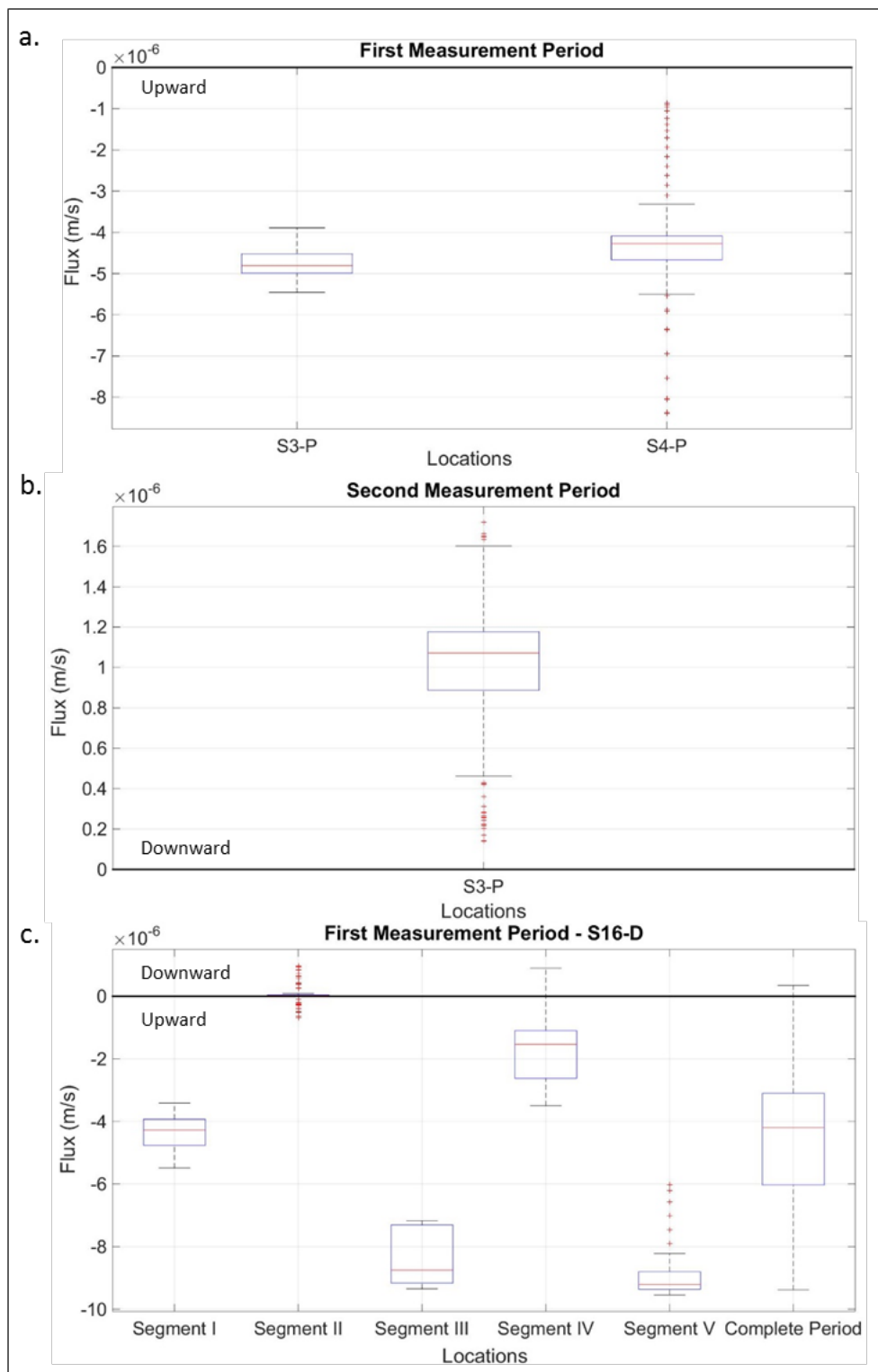


**Figure 9.** Box-plots summarizing vertical flux values calculated (a) for sites S3-P and S4-P during 16–25 March 2015 period; (b) for site S3-P during 12 July–2 August 2015; and (c) for site S16-D during 16 March–27 April 2015 period. Note that time segments indicating reservoir operation periods are shown in Figure 8b.

To observe the effect of reservoir water release on the vertical fluid fluxes at site S16-D, temperature time series were divided into five segments and flux values were calculated for each segment separately

(Figure 9c). The influence of the reservoir operation on the magnitude and direction of the exchange fluxes at site S16-D is clearly seen in Figure 9c. During normal conditions, when the reservoir holds water, (Segments I–III–V) the flux values are negative, indicating upwelling water. The magnitude of the upwelling flux becomes more negative from March towards the end of April (wetter towards drier periods). During the first water release period (Segment II), the average vertical flux value approaches zero with individual flux measurements narrowly spreading towards both positive and negative values, indicating a change in the reach character controlled by the surface water stage. The second water release period (Segment IV) is also marked by the significant decrease in the magnitude of the upwelling flux. In summary, this analysis indicates that reservoir operation has a significant effect on the variation in magnitude and direction of the vertical flux values at the study reach.

4.5. Seasonal Variation of Temperature and Electrical Conductivity Values along the Study Reach

4.5.1. Temperature

Variations in water temperature for stream water and piezometers at the monitoring locations are shown in Figure 10a. Note that the water temperature for the piezometers were measured at the mid-point of the perforated sections (see Section 3.2).

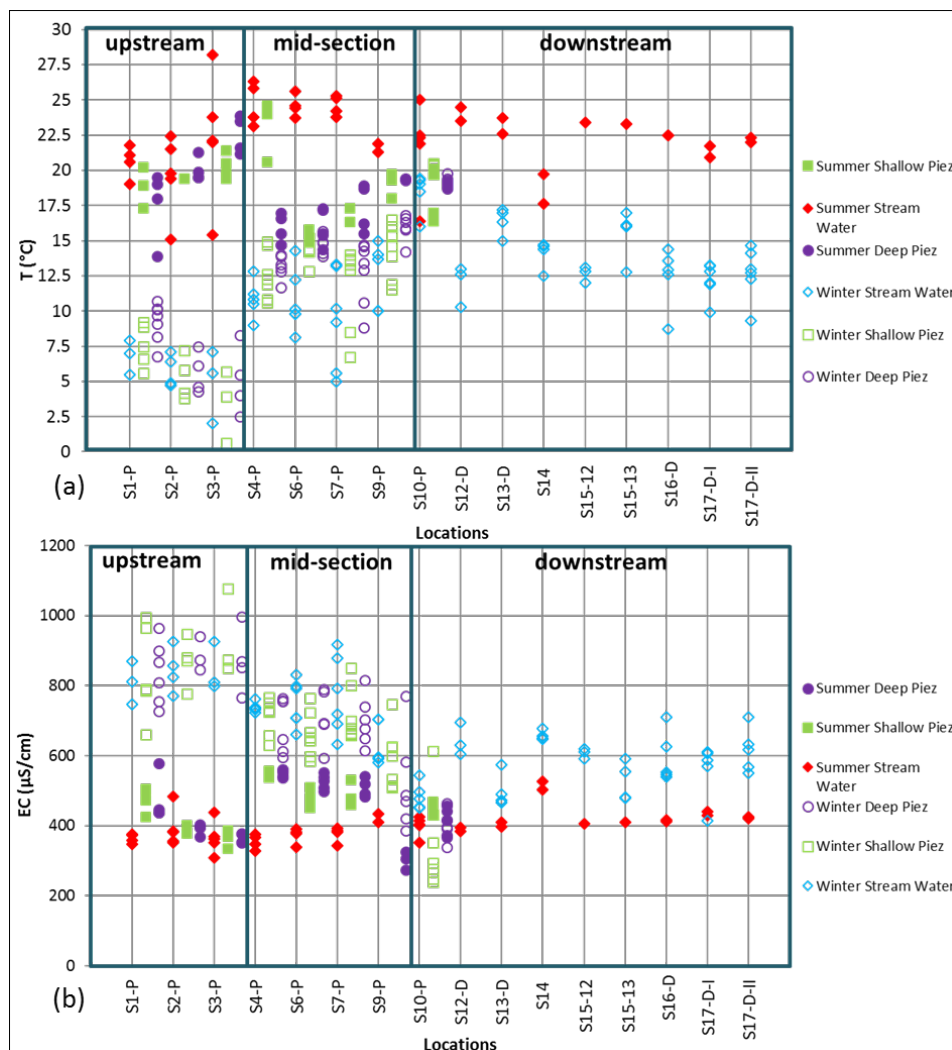


Figure 10. Variation in (a) temperature (b) EC values for stream water and piezometers at the monitoring locations.

Focusing on the summer season, stream water temperatures show a consistent increasing trend from S1-P through S4-P followed by a consistent decreasing trend downstream. The increasing temperature trend in stream water between S1-P and S4-P is possibly due to warming of the water released from the reservoir as it travels downstream in summer. The decreasing temperature trend from S4-P towards downstream is possibly due to the cooling effect of the upwelling groundwater. In winter, the stream water temperature shows similar behavior, but the trend was reversed due to colder air temperatures, supporting the same reasoning provided for the summer season. At upstream sites, S1-P, S2-P and S3-P piezometer water temperatures are similar to the stream water and both show significant seasonal fluctuations, supporting again the losing character of this stream reach. However, the temperatures of stream water and piezometers are significantly different from each other at the mid-section of the study reach (S4-P, S6-P, S7-P, S9-P), and while stream water temperatures fluctuate seasonally, piezometer temperatures show less fluctuation due to dampening by upwelling groundwater. In winter, this situation is less pronounced possibly due to reversals in the direction of streambed fluxes. Note that seasonal fluctuations in stream water and piezometers are less pronounced for S9-P and S10-P due to the increasing contribution of upwelling groundwater. For example, stream water temperature reaches its maximum value of 19.3 °C at site S10-P in winter due to the significant contribution by the warmer groundwater.

#### 4.5.2. Electrical Conductivity (EC)

Variation in electrical conductivity values for the stream water and piezometers (at the mid-screen level) are given in Figure 10b. It can be seen that the EC values of the stream water are higher in winter and lower in summer. The seasonal differences in the stream water EC values are most significant at the upstream reach (S1-P, S2-P and S3-P) with values ranging between 750–1000  $\mu\text{s}/\text{cm}$  in winter and 300–400  $\mu\text{s}/\text{cm}$  in summer. Notice that the EC values in the piezometers are similar to those of stream water and both show significant seasonal fluctuations indicating downwelling flux (losing reach) in the upstream reach. At the mid-section (S4-P through S9-P), summer EC values in the piezometers are significantly higher than those of surface water (with the exception of S9-P) and the difference becomes less pronounced through the downstream. At site S10-P, the difference in EC values between surface water and piezometers is less pronounced due to strong upwelling groundwater. At the mid-section, winter EC values in the piezometers and surface water are similar, possibly indicating that the reach turns into a losing stream in winter season. Note that the EC values shows a general increasing (decreasing) trend in summer (winter) due to the contribution of groundwater towards downstream.

#### 4.6. Chloride Mass Balance

Chloride concentrations and discharge values were measured for the sampling locations on date 4 August 2015. Solute mass balance was then applied to understand groundwater—stream interaction along the study reach.

Sites S12-D and S13-D join to form S15 and later flow towards S16-D (see Figure 2). Discharge at S16-D is significantly greater than the total discharge amount at S12-D and S13-D. The difference corresponds to 30.1 L/s. To find the source of this excess water, the following mass balance equation was written:

$$Q_{12} \times C_{12} + Q_{13} \times C_{13} + [Q_{16} - (Q_{12} + Q_{13})] \times C_{\text{excess water}} = Q_{16} \times C_{16} \quad (4)$$

$C_{\text{excess water}}$  was calculated as 19.0 mg/L. This chloride concentration is similar to that measured at site S13-D. Therefore, the excess water possibly seeps into the streambed upstream of S13-D and later emerges before S16-D. Another mass balance equation was formulated between S17-D and S16-D with a discharge difference of 11.4 L/s:

$$Q_{17} \times C_{17} = Q_{16} \times C_{16} + 11.4 \times C_{\text{excess water}} \quad (5)$$

Chloride concentration was found as 28.5 mg/L and this corresponds to the chloride concentration of upstream of the study reach. Therefore, downwelling stream water in the upstream section may reach the surface between sites S16-D and S17-D. These mass balance analysis shows that there are local flow systems within the boundaries of the study reach.

Chloride concentrations measured at site S10-P (immediate upstream, downstream and in the piezometer)—which is a groundwater discharge zone—are significantly lower compared to the chloride concentrations of the remaining sites. The chloride concentration through S2-P, S4-P and S6-P range between 27.8 mg/L and 33.5 mg/L. However, chloride concentrations in S10-P ranges between 6.9 mg/L and 7.4 mg/L. The effect of this low chloride concentration can be observed in the monitoring sites located at the downstream of S10-P. Site S13-D is situated just downstream of S10-P and has a lower chloride concentration (19.9 mg/L) than the chloride concentration of S12-D (28.7 mg/L), reflecting the characteristics of upstream of the study reach. Due to the merging of two different stream branches having different characteristics (S12-D and S13-D merge and form S15 and then flow towards S16-D), the chloride concentrations of S16-D and S17-D are between the chloride concentrations of sites S12-D and S13-D. This demonstrates the effect of S10-P at the more downstream sites of the study reach.

The chloride concentrations measured in the study reach were compared with those measured in nearby wells to infer possible connections between the groundwater feeding the study reach and the surrounding aquifer systems. Yazıcıgil et al. [32] reported chloride concentrations in wells located near the study reach. According to Yazıcıgil et al. [32], the chloride concentrations in wells representing the deep volcanic units (PW1, PW4A) range between 143 mg/L and 261 mg/L, which are significantly higher compared to those measured in the study area. These wells represent the volcanics that have deeper flow systems [32] with long residence times; hence, the significantly high chloride concentrations. A shallow well, CEL 52, has a lower chloride concentration (35.5 mg/L) compared to PW1 and PW4A, because this well represents volcanics characterized by a shallow flow system [32]. Cavuslar and Kocalar units have lower chloride concentrations compared to the volcanics. Also, PW3 (3.1 mg/L) screened in both Aktepe and Kocalar units has a noticeably low chloride concentration. It was found that chloride concentrations in S6-P are close to values of the shallow groundwater system that interacted with volcanics. In addition, S10-P showed similar chloride concentration values with groundwater sampled from wells drilled in the sedimentary rocks of Lower Cavuslar units (CEL44 and CEL51), representing the deeper confined aquifer. Chloride concentrations in CEL44 and CEL51 are 7.1 mg/L and 7.9 mg/L, respectively. Thus, it can be concluded that the groundwater from the deeper confined aquifer is seeping through the streambed at this location under the control of the nearby fault systems.

## 5. Discussion

This section provides a synthesis of the results obtained from various elements of the proposed methodology to understand the spatio-temporal variability of the exchange processes along the study reach. Strengths and limitations of the methods utilized are also discussed.

### 5.1. Spatio-Temporal Variability of the Exchange Processes

The methods utilized in the multi-scale framework pointed out that the direction and magnitude of water exchange vary spatially and temporally along the study reach. Based on the VHG values, the study reach is classified into three broad sections; upstream losing section (S1-P, S2-P and S3-P), mid-section (S4-P, S6-P, S7-P and S9-P) with seasonally varying conditions and the gaining site S10-P. This means that groundwater contributions increase downstream along the study reach. This finding is supported by other observations as well. The results obtained from the discharge measurements agree well with the VHG values since discharge increases downstream due to groundwater contributions (Figure 7). Also, variations in streambed temperatures at locations S3-P, S4-P and S16-D indicate that S3-P is located in the losing reach (significant diurnal variations in streambed temperatures) and

S4-P and S16-D are under the influence of the upwelling water from the streambed (damped diurnal variations in streambed temperatures). In July–August 2015, S3-P is characterized by a downwelling flux in agreement with the vertical hydraulic gradient measurements. Note, however, that the VFLUX result is in contrast with the VHG measurements for this site for March 2015. This behavior is possibly due to the distance between the i-buttons and the piezometer location. VHG values discussed earlier in Figure 5 indicate that S4-P became a gaining reach starting from January 2015. This information is also supported by temperature-based negative vertical fluid flux values provided in Figure 9. For site S4-P, the flux directions calculated using VFLUX and piezometer observations are the same during March 2015. Seasonal variations in temperature and electrical conductivity values along the study reach support the VHG results; upstream, mid-section and S10-P are characterized by losing, losing-gaining and gaining characters respectively. Especially, the groundwater discharge zone S10-P is distinguishable. Seasonal fluctuations in stream water and piezometers are less pronounced for S10-P due to increasing contributions of upwelling groundwater. Also, the stream water temperature reaches its maximum value of 19.3 °C at site S10-P in winter due to the warmer groundwater contribution. The difference in EC values between surface water and piezometers is less pronounced due to strong upwelling groundwater at site S10-P.

According to streambed temperature and differential discharge measurements, the operation of the upstream Doganozu Dam has a significant effect on the exchange processes. The effect of reservoir operation is observed as a periodic change in the streambed temperature recorded by the temperature loggers installed at two different depths (Figure 8). During reservoir water release, the temperature at both depths approaches the air temperature because the effect of the surface water increases and the influence of upwelling flux decreases. Also, vertical flow directions in the reaches change and are controlled by surface water stage, resulting in a decrease in the magnitude of the upwelling flux. However, when the reservoir operation is halted, the streambed temperature difference at two depths is more pronounced, indicating less surface water head. Also, flux values become negative, indicating upwelling water. In addition, streambed temperature values at deeper sections become almost stable and show less diurnal variations compared to shallower sections. These findings are supported by the differential discharge measurements as well. The peak discharge values are observed during the release of reservoir water. When moving towards downstream, discharge values show an increase during normal conditions. However, the discharge amount measured in the most downstream site (S17-D) in the study reach is lower than the discharge measured at more upstream sites (S3-P, S15-D and S16-D) after the reservoir water release, because surface water stage increases during this period and the stream turns into a losing stream along the study reach. When the effect of reservoir water decreases, discharge in S17-D becomes higher again compared to the upstream sites.

As mentioned in Section 2.2, due to the normal faults (Kizilca Fault, Kirmir 2 Fault and Demircioren Fault) located to the south of the study reach (Figure 3), groundwater originating from the deeper confined aquifer (sedimentary rocks of Lower Cavuslar units) possibly reaches the surface at S10-P. Comparisons of chloride concentrations measured in the study reach with the nearby wells indicate that groundwater coming from a deeper confined aquifer system including sedimentary rocks of Lower Cavuslar units feed the Kirmir Stream at this location. In terms of chloride concentrations, S10-P can be distinguished from other sections of the study reach. For instance, the water originating from the shallow groundwater system that interacted with volcanics possibly surfaces at site S6-P. This distinguishable character of S10-P is also supported by the other methods utilized. TIR imagery pinpoints the hotspot in S10-P and this site has the highest negative VHG magnitudes among all locations regardless of the season. Temperature and electrical conductivity variations support this finding as well. As mentioned, the temperature of stream water reaches the value of 19.3 °C at this location in the winter season. Also, piezometer water temperatures show similar values for both seasons, indicating strong upwelling flux.

## 5.2. Strengths and Limitations of the Methods

Each method utilized in this study has its own strengths, limitations and uncertainties. TIR imagery was found to be an effective and efficient tool in rapid identification of both groundwater seepage locations in shallow surface water and the temperature differences between merging channels over large areas. However, for the thermal camera to be useful, the signature of the groundwater seepage from the streambed should be identifiable at the skin of the surface water, which is generally the case for shallow water depths. In our case, the stream water depth varied between 4.5 cm and 15.5 cm during TIR analysis. In addition, shadow effect, reflection and vegetation cover over the stream water should be carefully eliminated for the TIR images to be useful. We recommend tandem operation of TIR camera and a regular camera over a handheld platform viewing the same scene for this task.

The uncertainty in stream discharge measurements increases with increasing discharge due to turbulence and representativeness issues with velocity measurements. Hence, discharge measurements for high flows are expected to have more errors; such as the case during reservoir release. The vertical water flux values derived from streambed temperature profiles are based on the assumption that the flow at the interface between stream and streambed can be characterized as one-dimensional and in the vertical direction. Although we expect the water movement at the interface in fact to be complex (three dimensional), the flux values derived with this method still provide valuable information on the rate of exchange process.

The hierarchical, multi-scale framework outlined in this study enabled cost-effective and efficient identification and quantification of spatially and temporally variable surface water-groundwater exchange processes along the study reach. Geologic and geomorphologic information at the regional scale helped to identify stream reaches with surface water-groundwater interaction potential hence enabled efficient (through reducing labor time and cost) transition to the smaller scale investigations. Without the TIR imagery, it would not be possible to rapidly identify groundwater discharge locations along the shallow stream reach. Differential discharge and nested piezometer measurements were valuable to quantify additions/losses along the reach and the direction of the streambed exchange fluxes, respectively, during field campaigns. Streambed temperature loggers were valuable in further quantifying the direction and the magnitude of the exchange processes at finer time scales in a continuous manner. Chloride concentrations shed further light on the source aquifers. Hence, the value of the proposed framework lies in the incorporation of information gathered at the larger scales to guide measurements at the smaller scale. Note that the application of multiple methods at a hierarchy of scales also help to cross check the information obtained from a specific method with others and hence improves our understanding of groundwater—surface water interaction processes.

Our recommendations for improving the methodology outlined in this study include increasing the number of independent measurements such as major ion chemistry and environmental tracers; i.e., Radon 222 [38] together with implementation of a numerical model, to better characterize the exchange processes. Instrumentation enabling continuous monitoring of water levels and temperature in the surface water and the piezometers is expected to shed further light in the temporal variation of the exchange processes. Our study indicated that the reservoir operation has a significant impact on the direction and magnitude of the exchange processes at the interface due to stream stage fluctuations; a similar finding was also reported by Binley et al. [39], Southern & Binley [40] and Anibas et al. [9]. Hence, further studies focusing on the hydraulic gradient reversals due to reservoir operation with possible significance for biogeochemistry and ecology of the hyporheic zone and the stream corridor are needed.

## 6. Conclusions

The exchange processes at the groundwater-surface water interface are complex, scale-dependent and hence difficult to characterize. The hierarchical, multi-scale methodology outlined in this study allows for characterization of these multi-scale processes in an efficient and effective manner.

The proposed methodology was applied to characterize the interaction between surface water and groundwater along a 2-km reach in Kirmir stream—a controlled stream in Ankara, Turkey. The methodology started with utilizing geological and geomorphological information at the regional scale to identify locations of potentially significant interaction between groundwater and surface water. Utilizing this regional scale information, the study area was selected as the location characterized by breaks in streambed slope and close to three major faults. Moving to the reach scale, thermal infrared imagery (TIR) was utilized to pinpoint the locations where groundwater seepage occurs within the streambed. TIR imagery was helpful in determining a major groundwater seepage zone that coincides with the nearby fault system. Based on these larger scale and rapid investigations, we planned the locations for point scale measurements including nested piezometers for observing vertical hydraulic gradient and vertical streambed temperature profiles to calculate the vertical fluid fluxes at fine temporal scale. Longitudinal profiles of temperature and electrical conductivity were measured along the reach. Differential discharge measurements taken during baseflow conditions helped us to understand the gains/losses through the streambed. Analysis of the point-scale measurements together with the differential discharge measurements indicated that the stream reach can be separated into three distinct sections; upstream section with losing character, downstream section with gaining character and mid-section with a seasonally variable character. Variation in streambed elevation throughout the study reach was found to have an important control on the vertical exchange processes. Moreover, our results indicated that the operation of the upstream Doganozu Dam has a strong impact on both the magnitude and the direction of vertical water exchange along the streambed. Analysis of chloride concentrations measured from piezometers, surface water and nearby wells indicated that the groundwater from the shallow groundwater system interacted with volcanics seeps into the streambed at the mid-section. Moreover, the lower confined aquifer system is likely the source of the groundwater inflow to the streambed at a fault-controlled location. Although each measurement methodology is inherently uncertain (see Section 5), including multiple types of measurements can be viewed as an independent check on the accuracy of the results.

**Author Contributions:** D.V. conducted the field work, analyzed the data and wrote the original draft paper. K.K.Y. designed and supervised the entirety of the field work and data analysis, helped in field work and reviewed/edited the draft paper.

**Funding:** This research was supported by a Middle East Technical University (METU) BAP Project BAP-08-11-2013-064. The first author received a scholarship from the Scientific and Technological Research Council of Turkey (TÜBİTAK Program No: 2210-C).

**Acknowledgments:** The authors are thankful to the Hydrochemistry Laboratory of Hacettepe University for the analysis of Chloride concentrations.

**Conflicts of Interest:** The authors declare no conflict of interest.

## References

1. Tóth, J. A conceptual model of the groundwater regime and the hydrogeologic environment. *J. Hydrol.* **1970**, *10*, 164–176. [[CrossRef](#)]
2. Winter, T.C.; Harvey, J.W.; Franke, O.L.; Alley, W.M. *Ground Water and Surface Water A Single Resource*; Circular 1139; U.S. Geological Survey: Reston, VA, USA, 1998.
3. Sophocleous, M. Interactions between groundwater and surface water: The state of the science. *Hydrogeol. J.* **2002**, *10*, 52–67. [[CrossRef](#)]
4. Brodie, R.; Sundaram, B.; Tottenham, R.; Hostetler, S.; Ransley, T. *An Adaptive Management Framework for Connected Groundwater-Surface Water Resources in Australia*; Bureau of Rural Sciences: Canberra, Australia, 2007; p. 179.
5. Hancock, P.J.; Boulton, A.J.; Humphreys, W.F. Aquifers and hyporheic zones: Towards an ecological understanding of groundwater. *Hydrogeol. J.* **2005**, *13*, 98–111. [[CrossRef](#)]
6. Findlay, S. Importance of surface-subsurface The hyporheic zone exchange in stream ecosystems. *Limnol. Oceanogr.* **1995**, *40*, 159–164. [[CrossRef](#)]

7. Woessner, W.W. Stream and fluvial plain ground water interactions: Rescaling hydrogeologic thought. *Groundwater* **2000**, *38*, 423–429. [[CrossRef](#)]
8. Humphreys, W.F. Hydrogeology and groundwater ecology: Does each inform the other? *Hydrogeol. J.* **2009**, *17*, 5–21. [[CrossRef](#)]
9. Anibas, C.; Verbeiren, B.; Buis, K.; Chormański, J.; de Doncker, L.; Okruszko, T.; Meire, P.; Batelaan, O. A hierarchical approach on groundwater-surface water interaction in wetlands along the upper Biebrza River, Poland. *Hydrol. Earth Syst. Sci.* **2012**, *16*, 2329–2346. [[CrossRef](#)]
10. Triska, F.; Duff, J.; Avanzino, R. The role of water exchange between a stream channel and its hyporheic zone in nitrogen cycling at the terrestrial—Aquifer interface. *Hydrobiologia* **1993**, *251*, 167–184. [[CrossRef](#)]
11. Constantz, J. Interaction between stream temperature, streamflow, and groundwater exchanges in alpine streams. *Water Resour. Res.* **1998**, *34*, 1609–1615. [[CrossRef](#)]
12. Winter, T.C.; Rosenberry, D.O. The interaction of ground-water with prairie pothole wetlands in the Cottonwood Lake area, east-central North Dakota, 1979–1990. *Wetlands* **1995**, *15*, 193–211. [[CrossRef](#)]
13. Winter, T.C. Relation of streams, lakes, and wetlands to groundwater flow systems. *Hydrogeol. J.* **1999**, *7*, 28–45. [[CrossRef](#)]
14. Harvey, J.W.; Bencala, K.E. The Effect of Streambed Topography on Surface-Subsurface Water Exchange in Mountain Catchments. *Water Resour. Res.* **1993**, *29*, 89–98. [[CrossRef](#)]
15. Peterson, E.W.; Sickbert, T.B. Stream water bypass through a meander neck, laterally extending the hyporheic zone. *Hydrogeol. J.* **2006**, *14*, 1443–1451. [[CrossRef](#)]
16. Bencala, K.E.; Gooseff, M.N.; Kimball, B.A. Rethinking hyporheic flow and transient storage to advance understanding of stream-catchment connections. *Water Resour. Res.* **2011**, *47*. [[CrossRef](#)]
17. Morrice, J.A.; Valett, H.M.; Dahm, C.N.; Campana, M.E. Alluvial Characteristics, Groundwater–Surface Water Exchange and Hydrological Retention in Headwater Streams. *Hydrol. Process.* **1997**, *11*, 253–267. [[CrossRef](#)]
18. Wroblecky, G.; Campana, M.; Valett, H.; Dahm, C. Seasonal variation in surface-subsurface water exchange and lateral hyporheic area of two stream-aquifer systems. *Water Resour. Res.* **1998**, *34*, 317–328. [[CrossRef](#)]
19. Fleckenstein, J.H.; Niswonger, R.G.; Fogg, G.E. River-aquifer interactions, geologic heterogeneity, and low-flow management. *Groundwater* **2006**, *44*, 837–852. [[CrossRef](#)] [[PubMed](#)]
20. Kalbus, E.; Reinstorf, F.; Schirmer, M. Measuring methods for groundwater, surface water and their interactions: A review. *Hydrol. Earth Syst. Sci. Discuss.* **2006**, *3*, 1809–1850. [[CrossRef](#)]
21. Kikuchi, C.P.; Ferré, T.P.A.; Welker, J.M. Spatially telescoping measurements for improved characterization of ground water–surface water interactions. *J. Hydrol.* **2012**, *446–447*, 1–12. [[CrossRef](#)]
22. Mouhri, A.; Flipo, N.; Rejiba, F.; de Fouquet, C.; Bodet, L.; Kurtulus, B.; Talleg, G.; Durand, V.; Jost, A.; Ansart, P.; et al. Designing a multi-scale sampling system of stream-aquifer interfaces in a sedimentary basin. *J. Hydrol.* **2013**, *504*, 194–206. [[CrossRef](#)]
23. Lee, D.R.; Hynes, H.B. Identification of groundwater discharge zones in a reach of Hillman Creek in southern Ontario. *Water Pollut. Res.* **1997**, *13*, 121–133.
24. Andersen, M.S.; Baron, L.; Gudbjerg, J.; Chapellier, D.; Jakobsen, R.; Gregersen, J.; Postma, D. Nitrate-rich groundwater discharging into a coastal marine environment. *J. Hydrol.* **2007**, *336*, 98–114. [[CrossRef](#)]
25. Cey, E.E.; Rudolph, D.L.; Gary, P.W.; Aravena, R. Quantifying groundwater discharge to a small perennial stream in southern Ontario, Canada. *J. Hydrol.* **1998**, *210*, 21–37. [[CrossRef](#)]
26. Murdoch, L.C.; Kelly, S.E. Factors affecting the performance of conventional seepage meters. *Water Resour. Res.* **2003**, *39*. [[CrossRef](#)]
27. Shinn, E.; Reich, C.; Hickey, T. Seepage Meters and Bernoulli's Revenge. *Estuaries* **2002**, *25*, 126–132. [[CrossRef](#)]
28. Andersen, M.S.; Acworth, R.I. Stream-aquifer interactions in the Maules Creek catchment, Namoi Valley, New South Wales, Australia. *Hydrogeol. J.* **2009**, *17*, 2005–2021. [[CrossRef](#)]
29. Hyun, Y.; Kim, H.; Lee, S.-S.; Lee, K.-K. Characterizing streambed water fluxes using temperature and head data on multiple spatial scales in Munsan stream, South Korea. *J. Hydrol.* **2011**, *402*, 377–387. [[CrossRef](#)]
30. Rosenberry, D.O.; Pitlick, J. Local-scale variability of seepage and hydraulic conductivity in a shallow gravel-bed river. *J. Hydrol.* **2009**, *23*, 3306–3318. [[CrossRef](#)]
31. Rojay, B. *Structural Evolution of Çeltikçi-Gümele Area during Post-Miocene*; Middle East Technical University: Ankara, Turkey, 2013.

32. Yazıcıgil, H.; Çamur, Z.; Yılmaz, K.K.; Sayıt, A.P.; Kahraman, C. *Development of Grounwater Flow Model for the Celtikci Coal Basin, Design of Dewatering and Assessment of Potential Impacts on Groundwater Resources* indirilmesi; Middle East Technical University: Ankara, Turkey, 2015.
33. Constantz, J.E.; Niswonger, R.G.; Stewart, A.E. Analysis of temperature gradients to determine stream exchanges with ground water. In *Field Techniques for Estimating Water Fluxes between Surface Water and Ground Water*; Geological Survey (U.S.): Reston, VA, USA, 2007; pp. 115–128.
34. Hatch, C.E.; Fisher, A.T.; Revenaugh, J.S.; Constantz, J.; Ruehl, C. Quantifying surface water-groundwater interactions using time series analysis of streambed thermal records: Method development. *Water Resour. Res.* **2006**, *42*. [[CrossRef](#)]
35. Anibas, C.; Schneidewind, U.; Vandersteen, G.; Joris, I.; Seuntjens, P.; Batelaan, O. From streambed temperature measurements to spatial-temporal flux quantification: Using the LPML method to study groundwater-surface water interaction. *Hydrol. Process.* **2015**. [[CrossRef](#)]
36. Vandersteen, G.; Schneidewind, U.; Anibas, C.; Schmidt, C.; Seuntjens, P.; Batelaan, O. Determining groundwater-surface water exchange from temperature-time series: Combining a local polynomial method with a maximum likelihood estimator. *Water Resour. Res.* **2015**, *51*, 922–939. [[CrossRef](#)]
37. Briggs, M.A.; Lautz, L.K.; Buckley, S.F.; Lane, J.W. Practical limitations on the use of diurnal temperature signals to quantify groundwater upwelling. *J. Hydrol.* **2014**, *519*, 1739–1751. [[CrossRef](#)]
38. Unland, N.P.; Cartwright, I.; Andersen, M.S.; Rau, G.C.; Reed, J.; Gilfedder, B.S.; Atkinson, A.P.; Hofmann, H. Investigating the spatio-temporal variability in groundwater and surface water interactions: A multi-technique approach. *Hydrol. Earth Syst. Sci.* **2013**, *17*, 3437–3453. [[CrossRef](#)]
39. Binley, A.; Ullah, S.; Heathwaite, A.L.; Heppell, C.; Byrne, P.; Lansdown, K.; Trimmer, M.; Zhang, H. Revealing the spatial variability of water fluxes at the groundwater-surface water interface. *Water Resour. Res.* **2013**, *49*, 3978–3992. [[CrossRef](#)]
40. Southern, M.D.; Binley, A. Temporal responses of groundwater-surface water exchange to successive stormevents. *Water Resour. Res.* **2015**, *51*, 1112–1126. [[CrossRef](#)]



© 2018 by the authors. Licensee MDPI, Basel, Switzerland. This article is an open access article distributed under the terms and conditions of the Creative Commons Attribution (CC BY) license (<http://creativecommons.org/licenses/by/4.0/>).